Supporting Information

Haddad et al. 10.1073/pnas.1716418115

X-Ray Measurements

The X-ray measurements comprised reflectivity (XR), GISAXS, and transmission-mode bulk SAXS. The scattering geometries for these methods are shown in Fig. S1. For all geometries, the wave vectors fulfill $|\vec{k}_{in}| = |\vec{k}_{out}| = 2\pi/\lambda$, where λ is the X-rays' wavelength, and the scattering vector is $\vec{q} = \vec{k}_{out} - \vec{k}_{in}$. We discuss here briefly only those features which are not available in standard textbooks (1–5), and which are required for the understanding the discussion in the main text.

X-Ray Reflectivity. The geometry for this method is shown in Fig. S1*A*. Since $\vec{q} = \vec{q}_z$ for this geometry, XR probes the laterally averaged surface-normal EDP, $\rho_e(z)$. XR measurements record the reflected intensity fraction, $R(q_z)$, of an X-ray beam incident on (and reflected from) the surface at a grazing angle α as a function of the surface-normal scattering vector $q_z = (4\pi/\lambda)\sin(\alpha)$.

Theory. $R(q_z)$ and $\rho_e(z)$ are related through the Born approximation for weak reflections by (1, 2)

$$R(q_z)/R_F(q_z) = \left| \rho_b^{-1} \int (\mathrm{d}\rho_e(z)/\mathrm{d}z) \exp(-iq_z z) \mathrm{d}z \right|^2, \qquad \textbf{[S1]}$$

where ρ_b is the bulk electron density, and $R_F(q_z)$ is the Fresnel reflectivity from an ideally flat and abrupt interface. To extract $\rho_e(z)$ from the measured $R(q_z)$, a physically motivated model for ρ_e is constructed, and the corresponding analytic $R(q_z)$ is calculated using Eq. **S1**. Fitting this calculated curve to the measured $R(q_z)$ yields the model-defining parameter values (6).

Model. We adopt here the modified DCM used successfully for layered liquid metal (7–10) and ionic liquid (11–14) interfaces,

$$\rho_e(z) = \rho_b \sum_{m=0}^{\infty} \frac{d}{\sigma_m \sqrt{2\pi}} \exp\left[-\frac{(z-md)^2}{2\sigma_m^2}\right] + \rho_a \frac{d}{\sigma_a\sqrt{2\pi}} \exp\left[-\frac{(z+d_0)^2}{2\sigma_a^2}\right]. \qquad \textbf{[S2]}$$

This model represents $\rho_e(z)$ by d-spaced layers of a Gaussian electron density distribution with an effective width $\sigma_m = \sqrt{\sigma_0^2 + m\bar{\sigma}^2}$. As m increases, the Gaussians broaden, reducing smoothly the oscillatory deviations of $\rho_e(z)$ from the bulk density ρ_b. Here σ_0 is the surface roughness (including the contributions from thermal capillary waves and any nonthermal intrinsic roughness), and $\bar{\sigma}$ controls the layering decay length by controlling the broadening of the Gaussians. The second term represents the enrichment of the layer of alkyl chains (at an average position d_0, a width σ_a, and density ρ_a) protruding from the first cation layer into the air.

Fits. The fits were conducted in two rounds. In the first round, all parameters of the model were free to vary, yielding good fits. The values of $\bar{\sigma}$ were found to be narrowly clustered around 7 Å for all $n \geq 6$, except $n = 20, 22$. For $n \leq 4$, ρ_a converged to 0, and $\bar{\sigma}$ decreased significantly with decreasing n, reaching $\bar{\sigma} \approx 2$ Å for $n = 2$. The $\bar{\sigma}$ decrease was accompanied by a concomitant decrease in d, to values close to $\bar{\sigma}$, rendering the resultant $\rho_e(z)$ devoid of modulations, and simple-liquid-like, as dictated by the shape of the measured $n \leq 4$ XR curves, discussed in the main text.

Based on the results of the first round, in the second round of fits for $n \leq 6$, a fixed $\rho_a = 0$ e/Å^3 was used and all parameters of the first term in Eq. **S2** were all allowed to vary. For $6 \leq n \leq 18$, a fixed $\bar{\sigma} = 7$ Å was used, and all other parameters, including those of the second term of Eq. **S2**, were allowed to vary. For $n = 20$ and 22, the fits obtained for $\bar{\sigma} = 7$ Å were poor. Thus, for these n, $\bar{\sigma}$ was also allowed to vary and yielded $\bar{\sigma} = 7.7$ and 7.4 Å, respectively. The values obtained from this round of fits are the ones shown and discussed in the main text. We also note that $n = 6$ constitutes a special case. Here the measured XR could be fit equally well either by fixing $\bar{\sigma} = 7$ Å and allowing d and ρ_a to vary, as for all $n \geq 6$, or by fixing $\rho_a = 0$ e/Å^3 and allowing d and $\bar{\sigma}$ to vary, as for all $n \leq 4$. Coinciding curves were obtained for the $n = 6$ XR fits and EDPs using the two methods. The curves shown for $n = 6$ in Fig. 1 *A* and *B* were obtained by the latter method.

GISAXS. The geometry for this measurement mode is shown in Fig. S1*B*. Here the detector is offset from the reflection plane *x–z* by an angle 2θ to pick up X-rays scattered with the scattering vector $\vec{q}$. As $\vec{q}$ now has a component in the horizontal *x–y* plane, it is sensitive to order in that plane. Thus, long-range surface-parallel order will produce sharp peaks, known as GID peaks, upon scanning 2θ. Such peaks were not found for any n or temperature in our measurements. An LL short-range order will produce broad diffuse peaks. When several different correlation distances D_n exist in the liquid, several diffuse rings with radii $q_n = 2\pi/D_n$ will be observed in the registration plane *y–z*. Circular averaging over the intensities in the registration plane yields, in that case, the GISAXS intensity patterns shown in Fig. 4, exhibiting two peaks, corresponding to two different correlation lengths D_n. The lowest-q peak of the bulk SAXS, denoted in Fig. 4 as Peak I (see below), was not accessible in the GISAXS geometry in our measurements.

It is important to note that the scattering volume sampled by the incident X-ray beam, and its vertical position, varies with α. An interface between two media of different refractive indices splits an incident beam into reflected and refracted beams. The RTILs' refractive index for X-rays is less than unity, while that of air is unity. Thus, by Snell's law of optics, an angle α_c exits for the RTIL–air interface such that, when $\alpha < \alpha_c$, the refracted beam becomes evanescent and penetrates only to a depth $\Lambda \approx [\lambda/(4\pi)]/\sqrt{\alpha_c^2 - \alpha^2}$ below the surface. When $\alpha > \alpha_c$, the refracted beam penetrates to macroscopic depths below the surface, and thus samples the RTIL's bulk. In our case, $\alpha_c = 0.057°$, and the GISAXS measurements were carried out below ($\alpha_1 = 0.045°$; Fig. 4, blue symbols) and above ($\alpha_2 = 0.15°$; Fig. 4, red symbols) α_c. These α yield, respectively, $\Lambda \approx 70$ Å, where predominantly the layered surface region is sampled, and a macroscopic penetration, where the bulk is sampled.

Transmission-Mode SAXS. The geometry for this case is shown in Fig. S1*C*. The incident beam travels along the x axis, and is scattered through the z-axis-oriented sample contained in a capillary, yielding, for a liquid, equal-q circles in the registration plane *y–z*. As for GISAXS, an LL short-range order will produce diffuse rings in this plane. When several different correlation distances D_n exist in the liquid, several diffuse rings with radii $q_n = 2\pi/D_n$ will be observed in the registration plane. Fixed-q circular averaging over the SAXS pattern yields an intensity versus q plot, such as that shown in black symbols in Fig. 4, with peak positions corresponding to the bulk correlation periods.

Melting Temperatures of Long-Chain RTILs

[C$_n$mim][NTf$_2$] RTILs with $n \geq 14$ melt above RT ($\sim$25 °C). Note, however, that, once molten, RTILs can be undercooled significantly, up to tens of degrees, and for long (cooling-dependent) times, before they solidify. Thus, it is possible to obtain liquid phases at RT even for some of the $n \geq 14$ RTILs. Melting temperatures T_m for $n = 12$ to 18 [literature values (15, 16)] and $n = 20$ to 22 [differential scanning calorimetry (DSC)-measured, at 5 K/min] are listed in Table S1.

1. Pershan PS, Schlossman ML (2012) *Liquid Surfaces and Interfaces: Synchrotron X-ray Methods* (Cambridge Univ Press, Cambridge, UK).
2. Als-Nielsen J, McMorrow D (2001) *Elements of Modern X-Ray Physics* (Wiley, New York).
3. Guinier A, Fournet G (1955) *Small-Angle Scattering of X-Rays* (Wiley, New York).
4. Feigin LA, Svergun DI (1982) *Small-Angle X-Ray Scattering* (Academic, New York).
5. Feigin LA, Svergun DI (1987) *Structure Analysis by Small-Angle X-Ray and Neutron Scattering* (Plenum, New York).
6. Ocko BM, et al. (1997) Surface freezing in chain molecules: Normal alkanes. *Phys Rev E* 55:3164–3182.
7. Magnussen OM, et al. (1995) X-ray reflectivity measurements of surface layering in liquid mercury. *Phys Rev Lett* 74:4444–4447.
8. DiMasi E, Tostmann H, Ocko BM, Pershan PS, Deutsch M (1998) X-ray reflectivity study of temperature-dependent surface layering in liquid Hg. *Phys Rev B* 58:R13419–R13422.
9. Elsen A, et al. (2010) Surface layering at the mercury-electrolyte interface. *Phys Rev Lett* 104:105501.
10. Elsen A, et al. (2013) In situ X-ray studies of adlayer-induced crystal nucleation at the liquid–liquid interface. *Proc Natl Acad Sci USA* 110:6663–6668.
11. Mezger M, et al. (2008) Molecular layering of fluorinated ionic liquids at a charged sapphire (0001) surface. *Science* 322:424–428.
12. Nishi N, et al. (2010) Ionic multilayers at the free surface of an ionic liquid, trioctyl-methylammonium bis(nonafluorobutanesulfonyl)amide, probed by X-ray reflectivity measurements. *J Chem Phys* 132:164705.
13. Mezger M, Ocko BM, Reichert H, Deutsch M (2013) Surface layering and melting in an ionic liquid studied by resonant soft X-ray reflectivity. *Proc Natl Acad Sci USA* 110:3733–3737.
14. Mezger M, et al. (2015) Solid-liquid interfaces of ionic liquid solutions: Interfacial layering and bulk correlations. *J Chem Phys* 142:164707.
15. Zhang S, Sun N, He X, Lu X, Zhang X (2006) Physical properties of ionic liquids: Database and evaluation. *J Phys Chem Ref Data* 35:1475–1517.
16. Bradley AE, et al. (2002) Small-angle X-ray scattering studies of liquid crystalline 1-alkyl-3-methylimidazolium salts. *Chem Mat* 14:629–635.

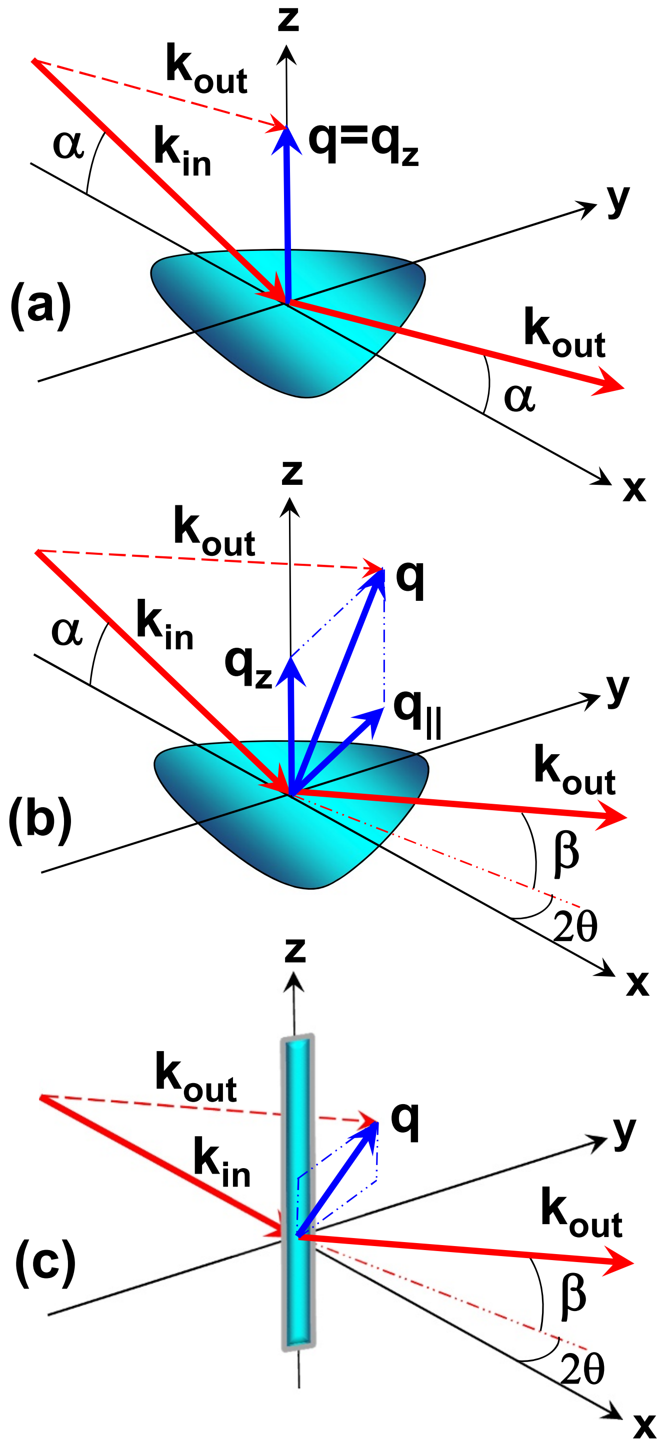

Fig. S1. X-ray scattering geometries for the methods discussed in the *X-Ray Measurements*. (*A*) Geometry of X-ray reflectivity (XR). (*B*) Geometry of grazing incidence X-ray diffraction (GISAXS). (*C*) Geometry of transmission-mode small-angle X-ray scattering (SAXS).

Table S1. Melting temperatures T_m of $[C_n mim][NTf_2]$ RTILs

n	T_m(°C)
12	16.7
14	34.3
16	42.1
18	44.8
20	57.7
22	65.7